INORGANIC CHEMISTRY
FRONTIERS

RESEARCH ARTICLE

View Article Online
View Journal | View Issue



Cite this: *Inorg. Chem. Front.*, 2024, **11**, 6880

# Cobalt and lithium recovery from spent $LiCoO_2$ using a free-standing potassium zinc hexacyanoferrate/carbon cloth composite electrode†

Mengxiang Ye, Huaimeng Li,* Xi Wu, Guofeng Zhang and Yunxia Zhang *

Rapid rejuvenation and extensive utilization of mobile electronic devices lead to the excessive accumulation of waste lithium-ion batteries (LIBs), specifically spent $LiCoO_2$ cathode materials. Considering the shortage of metal resources and the surging price of raw materials in the battery industry, an efficient strategy for selectively extracting valuable metals from spent $LiCoO_2$ is urgently required. Herein, nanocube-like potassium zinc hexacyanoferrate (denoted as KZHCF) was successfully fabricated on a carbon cloth (CC) substrate for selective $Co^{2+}$ adsorption from a spent $LiCoO_2$ cathode *via* the combination of simple electrodeposition and hydrothermal treatment. Under optimal operational conditions, 98.6% of $Co^{2+}$ was effectively extracted within 120 min at a constant potential of −0.4 V (*vs.* Ag/AgCl) with the CC/KZHCF composite as the working electrode, accompanied with a $Co^{2+}$ electrosorption capacity of 130.9 mg $g^{-1}$. Further, lithium ions in the electrolyte were separated and recovered in the form of $Li_2CO_3$ *via* simple chemical precipitation, highlighting the feasibility of the developed electrochemical system toward cobalt and lithium recovery. Significantly, the CC/KZHCF electrode materials could be regenerated through simple potential inversion, while adsorbed $Co^{2+}$ ions were facilely desorbed from the electrode surface and recovered as $Co(OH)_2$. This work will provide a meaningful guidance for the separation and recovery of various metals from waste LIBs.

Received 12th July 2024,
Accepted 21st August 2024

DOI: 10.1039/d4qi01752h

rsc.li/frontiers-inorganic



## 1. Introduction

LIBs have been rapidly progressing since their first commercial utilization in the 1990s and have gradually become the current mainstream energy storage batteries applied in the transport sector and portable electronic devices due to their excellent physicochemical characteristics, including light weight, long cycling lifespan and high energy density per unit weight.[1–4] As a typical representative, $LiCoO_2$ is the most commonly used cathode material in laptops, mobile phones, digital cameras and other devices.[5,6] With the increasingly rapid upgradation of electronic products in the information age, numerous obsolete electronics become e-waste and are not recycled properly. It is reported that the total global e-waste is expected to reach 65.3 million tons by 2025, including 464 000 tons of waste LIBs.[7,8] Considering the increasing market demand for important industrial raw materials, such as lithium, cobalt, and nickel, and the potential human health problems caused by the pollution from waste LIBs, the recovery of high value metals from spent LIBs is of great importance from both economic and environmental perspectives.[9]

The recycling and recovery of cobalt from waste LIBs usually begins with the pre-treatment process of physical separation for obtaining metal parts, including mechanical, mechanochemical and thermal dissolution methods.[10] Subsequently, the conventional technologies for metal recovery can be divided into hydrometallurgy, pyrometallurgy and their combinations.[11] Hydrometallurgical treatment comprises acid leaching and chemical precipitation processes. Inorganic and organic acids together with a reducing agent (*e.g.*, $H_2O_2$) are usually employed to dissolve electrode material powders, followed by chemical precipitation for direct metal recovery.[12] Pyrometallurgical technique involves high-temperature treatment for melting and reducing metallic components.[13] Given that these techniques are characterized by massive chemical reagent use, high energy consumption associated with acid-containing wastewater discharge and toxic gas emission leading to secondary pollution, an alternative economical and environmentally friendly method is in urgent demand for cobalt recovery.[14]

In addition to traditional ion separation techniques including adsorption,[15] chemical precipitation,[16] ion exchange,[17]

*Key Laboratory of Materials Physics, Centre for Environmental and Energy Nanomaterials, Anhui Key Laboratory of Nanomaterials and Nanotechnology, Institute of Solid State Physics, Institutes of Physical Science, Chinese Academy of Sciences, Hefei 230031, China. E-mail: hmli@issp.ac.cn, yxzhang@issp.ac.cn*

† Electronic supplementary information (ESI) available. See DOI: https://doi.org/10.1039/d4qi01752h

and membrane separation,[18] electrochemical sorption process[19] or capacitive deionization (CDI),[20] as an advanced technology was first proposed in the 1990s for removing salt ions from water. The target ions can be adsorbed when the electrode is charged and then also can be released to the bulk solution from the electrode material with short circuit or applied voltage reversal treatment.[21] With the rapid development of CDI technology, the target ions have expanded from the initial alkali metal ions ($K^+$, $Ca^{2+}$, $Na^+$, $Mg^{2+}$) to some heavy metals ($Cr^{3+}$, $Cd^{2+}$, $Pb^{2+}$, $Hg^{2+}$) and rare metals ($Li^+$, $Cs^+$, $Be^{2+}$, $Ti^{4+}$).[22,23] Traditional carbon-based materials, including activated carbon, graphene and carbon aerogel, have been applied as typical CDI electrodes due to their good electrical conductivity and high surface area.[24] However, the mechanism of storing ions in the electrical double layer (EDL) at the interface limits the application of carbon materials in complicated systems due to their poor selectivity and low removal capacity.[25] Hence, the design of novel electrode materials with high selectivity and outstanding performance during the adsorption/desorption cycles has been the focus of current CDI research.

Compared to the traditional carbon-based materials, which rely on the EDL mechanism to adsorb ions, the faradaic system with redox-active materials as the electrode with the merits of ion selectivity and high specific capacity is an alternative promising platform for environmental remediation.[26] Transition metal hexacyanoferrates (TMHCFs), or Prussian blue and its derivatives (PBAs), as typical redox-active materials, usually feature a face-centred cubic lattice structure and an open framework, facilitating the rapid insertion and extraction of cations from the aqueous solution.[27] Zinc hexacyanoferrate (ZnHCF), as one of the most chemically stable and low toxicity PBA analogues, has been widely applied in the field of aqueous rechargeable batteries. For instance, Niu *et al.* synthesized rhombohedral ZnHCF microcubes for high-voltage rechargeable sodium-ion batteries with high voltage output of 1.6 V and energy density of 59 W h $kg^{-1}$.[28] In another demonstration, Lu *et al.* modified ZnHCF nanocubes with the encapsulation of $MnO_2$ nanosheets for an enhanced reversible capacity of 75 mA h $g^{-1}$ at 1000 mA $g^{-1}$.[29] In addition to the applications as battery materials, ZnHCF has recently been used for the enrichment of radioactive elements from nuclear waste. Kim *et al.* developed a ZIF-8-derived ZnHCF composite for the enrichment of cesium ions from nuclear waste with a large $Cs^+$ uptake capacity (204.9 mg $g^{-1}$) and high selectivity towards a Na/Cs molar ratio of 1330.[30] Considering the advantage of high adsorption capacity of ZnHCF materials toward cations, it is of considerable interest to utilize ZnHCF to extract Co element from waste $LiCoO_2$ cathode materials.

In this work, the free-standing CC/KZHCF composite was synthesized through a simple electrodeposition and subsequent hydrothermal treatment for selective Co recovery from waste $LiCoO_2$ batteries. As expected, the resulting binder-free CC/KZHCF composite can be directly employed as the working electrode, achieving excellent $Co^{2+}$ adsorption/desorption capability. It is noteworthy that the sizes of KZHCF nanocubes can be modulated by varying the hydrothermal treatment time, thus giving rise to different $Co^{2+}$ extraction efficiencies. The impact of several crucial factors, including applied potentials, solution pH, stability and reusability of CC/KZHCF, is evaluated during the $Co^{2+}$ electrosorption process. Moreover, the plausible mechanism of $Co^{2+}$ insertion/extraction behaviour in KZHCF is revealed by analyzing the variation in the valence of metal species before and after electrosorption.

## 2. Experimental section

### 2.1 Materials and characterization

The waste laptop $LiCoO_2$ battery was purchased from the local electronic second-hand market. CC (0.34 mm in thickness) with 1.1 mΩ $cm^{-2}$ through plate resistance was obtained from Shanghai Hesen Electric Co., Ltd (Shanghai, China). Hydrochloric acid (HCl, 36.0–38.0%), hydrogen peroxide ($H_2O_2$, ≥30.0%), ammonium hydroxide ($NH_3{\cdot}H_2O$, 25.0–28.0%), zinc sulfate heptahydrate ($ZnSO_4{\cdot}7H_2O$, ≥99.5%) and sodium sulfate ($Na_2SO_4$, ≥99.0%) were purchased from Sinopharm Chemical Reagent Co., Ltd. Boric acid ($H_3BO_3$, ≥99.5%) and potassium ferricyanide ($K_3[Fe(CN)_6]$, ≥99.0%) were purchased from Aladdin Biochemical Technology Co., Ltd (Shanghai, China). The morphologies of the as-synthesized samples were characterized by scanning electron microscopy (SEM, SU-8020, Hitachi, Japan) and high-resolution transmission electron microscopy (HRTEM, JEM-2010, JEOL, Japan). X-ray diffraction patterns were recorded using an X-ray diffractometer (XRD, Panalytical Co., Netherland) with Cu Kα radiation. The chemical compositions and valence states of the surface elements of the samples were investigated by X-ray photoelectron spectroscopy (XPS, ESCALAB 250Xi, Thermo Scientific, USA) using Al-Kα radiation. The metal ions' concentration was monitored using inductively coupled plasma optical emission (ICP-OES, Thermo Fisher Scientific ICP6300, USA) spectrometry. All electrochemical experiments were powered by a CHI 660E workstation (Chenhua, China).

### 2.2 Leaching experiment

The waste laptop $LiCoO_2$ battery was first fully discharged in a 5% NaCl solution and then manually disassembled in the vacuum glove box. The cathode materials were obtained and subsequently crushed and sieved for pure $LiCoO_2$ powder. The leaching process was performed in a 100 mL beaker with 50 mL of mixed solution containing 2.5 M HCl and 0.6% (v/v) $H_2O_2$, in which 2.5 g of $LiCoO_2$ powder was added into the above solution and stirred for 48 h. Considering the higher reduction potential of $Co^{3+}$ than that of $H_2O_2$, the presence of $H_2O_2$ here was used to reduce $Co^{3+}$ to more soluble $Co^{2+}$. The leaching solution was then filtered using a PTFE membrane syringe filter with 0.22 μm pore size to remove any solid impurities for subsequent ICP-OES analysis and electrochemical adsorption experiments. The leaching reaction is based on the following equation (eqn (1)).[31]

$$6H^+ + H_2O_2 + 2LiCoO_2 \rightarrow 2Li^+ + 2Co^{2+} + 4H_2O + O_2 \quad (1)$$

### 2.3 Synthesis of the CC/KZHCF composite electrode

The CC/KZHCF composite electrode was fabricated through a simple electrodeposition and hydrothermal combination method according to the previous report with minor modifications.[32] The commercial CC (2 × 2 $cm^2$) was firstly treated with 3 M $HNO_3$ for 6 h at 80 °C to obtain better hydrophilicity, followed by drying in a 60 °C oven overnight and thorough rinsing with deionized (DI) water several times. Electrodeposition was conducted with a three-electrode apparatus. Typically, 50 mL aqueous solution containing 5 g of $ZnSO_4{\cdot}7H_2O$, 5 g of $Na_2SO_4$ and 1.6 g $H_3BO_3$ was used as the electrolyte. The hydrophilic CC, graphite rod and Ag/AgCl (saturated with KCl) electrodes were utilized as the working, counter and reference electrodes, respectively. The electrodeposition process was conducted under a constant current density of −50 mA $cm^{-2}$ for 600 s. The obtained CC/Zn electrode was rinsed with DI water and dried in a vacuum at 60 °C overnight. Subsequently, the as-prepared CC/Zn (with Zn coating area of 1 × 2 $cm^2$) electrode was added into a Teflon-lined stainless-steel autoclave containing 50 mL of 10 mM $K_3[Fe(CN)_6]$ and heated at 60 °C for various time durations. The obtained samples under different hydrothermal treatment times were labelled as CC/KZHCF-1 (5 h), CC/KZHCF-2 (7 h), CC/KZHCF-3 (9 h) and CC/KZHCF-4 (11 h). Unless otherwise specified, CC/KZHCF signifies the product obtained at 7 h of hydrothermal treatment. Finally, the CC/KZHCF electrodes were obtained after washing with DI water several times and dried in a 60 °C oven overnight. The synthetic reaction could be described with equation (eqn (2)).

$$3Zn + 6K_3[Fe(CN)_6] + 9H_2O = K_2Zn_3[Fe(CN)_6]_2 \cdot 9H_2O + 4K_4[Fe(CN)_6] \quad (2)$$

### 2.4 Electrochemical adsorption of cobalt

Cobalt adsorption experiments were conducted in a three-electrode system in which CC/KZHCF (1 × 2 $cm^2$), CC with the same area, and Ag/AgCl were utilized as the working electrode, counter electrode and reference electrode, respectively. The mixed solution containing $Co^{2+}$ and $Li^+$ was prepared by diluting the $LiCoO_2$ leaching solution 1000 times with DI water. In all experiments, the electrolyte volume was 50 mL and the pH was adjusted using 0.1 M HCl and $NH_3{\cdot}H_2O$. Before $Co^{2+}$ adsorption experiments, the CC/KZHCF electrode was firstly pretreated in 1 mg $L^{-1}$ $KNO_3$ solution at a working potential of +1.5 V (*vs.* Ag/AgCl) for 30 min to discharge the $K^+$ ions in the KZHCF and the residual $K^+$ during the synthesis. The relevant reaction is shown as follows (eqn (3)).[33]

$$K_4[Fe^{II}(CN)_6](\text{sorbent electrode}) \rightarrow 4K^+ + [Fe^{III}(CN)_6]^{3-} + e^- \quad (3)$$

After the elimination of $K^+$ ions, the CC/KZHCF electrode was transferred to the metal-containing solution for $Co^{2+}$ electrosorption. The electrosorption experiments were carried out when a fixed potential was applied on the working electrode and lasted for 120 min to reach an equilibrium state. 0.5 mL of the samples were withdrawn from the reactor at predetermined time intervals and filtered for subsequent metal concentration analysis by ICP-OES. The Co recovery efficiency was calculated using the following equation (eqn (4))

$$\text{Recovery efficiency} = \frac{C_0 - C_e}{C_e} \times 100\% \quad (4)$$

and the adsorption capacity on unit mass of CC/KZHCF ($Q$, mg $g^{-1}$), which was defined according to the following equation (eqn (5))

$$Q = \frac{(C_0 - C_e) \times V}{m} \times 100\% \quad (5)$$

where $C_0$ (mg $L^{-1}$), $C_t$ (mg $L^{-1}$) and $C_e$ (mg $L^{-1}$) stand for the initial, time $t$ and final concentration of metal ions, respectively. $V$ and $m$ are the solution volume and the weight of the CC/KZHCF electrode, respectively.

### 2.5 Cyclic experiments

After $Co^{2+}$ ions adsorption, the CC/KZHCF-Co electrode was washed with DI water and transferred to the $KNO_3$ (1 mg $L^{-1}$) electrolyte for $Co^{2+}$ ions desorption and electrode regeneration. An oxidation potential of +1.5 V (*vs.* Ag/AgCl) was applied on the CC/KZHCF-Co electrode for 30 min. After that, the regenerated electrode was washed with DI water and dried in an oven at 60 °C overnight for the next Co recovery experiment. The cyclic experiments were repeated for 5 rounds, and the concentration of $Co^{2+}$ ions was monitored by ICP-OES measurement.

## 3. Results and discussion

### 3.1 Fabrication of the CC/KZHCF composite electrode

Scheme 1 illustrates the fabrication process of the self-standing CC/KZHCF composite electrode, involving a simple electrodeposition and subsequent hydrothermal treatment. First, the commercial CC with hydrophilic surface was immersed into the electrolyte containing $ZnSO_4{\cdot}7H_2O$ as the precursor. In a three-electrode apparatus, Zn was *in situ* electrodeposited on the CC surface with a constant reduction potential at room temperature, generating a layer of Zn nanosheets. Subsequently, the as-obtained Zn nanosheets gradually grew into homogeneous KZHCF nanocubes through a redox reaction under the hydrothermal condition, in which metallic Zn can reduce $Fe^{3+}$ to $Fe^{2+}$ while it itself was oxidized to $Zn^{2+}$, accompanied by the for-

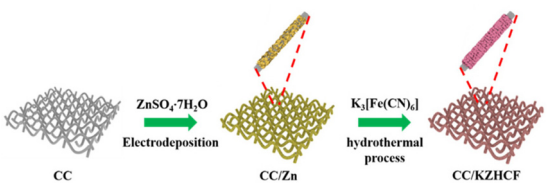


**Scheme 1** Schematic illustration of the preparation of the CC/KZHCF electrode.

mation of $K_2Zn_3[Fe(CN)_6]_2$ (KZHCF). As a consequence, KZHCF nanocubes align densely on the CC substrate to generate the CC/KZHCF composite. It should be mentioned that the size of the composite electrode can be easily scaled up on demand.

As a representative, the morphology of the as-prepared CC/KZHCF-2 composite was initially characterized by SEM observation. For CC/Zn, after electrodeposition, the entire textual surface of the CC substrate was covered uniformly with a layer of densely packed nanosheets with a lateral size of 1–2 μm (Fig. 1a), indicative of the uniform coating of Zn. In the subsequent hydrothermal process, these interconnected Zn nanosheets *in situ* transform to homogeneous KZHCF nanocubes in the $K_3[Fe(CN)_6]$ solution, which is well dispersed throughout the skeleton of the CC matrix (Fig. 1b). The microstructure of CC/KZHCF was further investigated by TEM observation. As displayed in Fig. 1c, these nanocubes possess a mean lateral dimension of 500 nm and a thickness of *ca.* 100 nm. Moreover, the corresponding elemental mapping images of a single KZHCF nanocube reveal that K, Zn, Fe, C and N elements are homogeneously distributed across the whole nanocube (Fig. 1d), confirming the successful fabrication of the CC/KZHCF composite. Further, the HRTEM image (Fig. 1e) demonstrates that the spacing of the interlayer lattice fringes can be identified as 5.4 Å and 4.1 Å, matching well with the (113) and (116) faces of $K_2Zn_3[Fe(CN)_6]_2{\cdot}9H_2O$ (JCPDS no. 33-1061), respectively.[34] Additionally, the hydrothermal treatment time plays a key role in the morphology of the fabricated CC/KZHCF composite. As demonstrated in Fig. S1,† the lateral dimension of KZHCF nanocubes gradually expands from 0.5 μm to 2 μm with increasing hydrothermal time, accompanied by a similar increase in the thickness. As a consequence, the loading masses of KZHCF nanocubes on CC substrate were calculated to be 8.5 mg, 11.3 mg, 18.8 mg and 24.2 mg for the as-fabricated CC/KZHCF-1, CC/KZHCF-2, CC/KZHCF-3, and CC/KZHCF-4 electrodes, respectively.

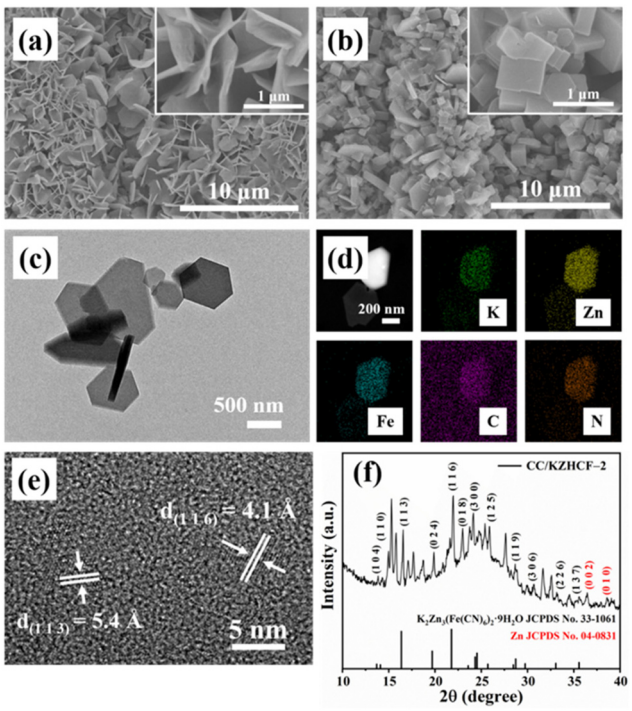


**Fig. 1** Morphological and structural characterization of the as-prepared samples: (a) SEM image of CC/Zn. (b) SEM image of CC/KZHCF-2. (c) TEM and (d) corresponding EDS elemental mapping of the KZHCF nanocubes. (e) HRTEM image of KZHCF; (f) XRD pattern of CC/KZHCF-2.

The crystalline phase of the as-prepared CC/KZHCF electrode was investigated by XRD (Fig. 1f). The diffraction peaks located at 36.3° and 39.0° are attributed to the (002) and (100) reflections from Zn nanosheets (JCPDS no. 04-0831), respectively.[35] Several main characteristic diffraction peaks at 16.4°, 19.7°, 21.8°, 24.3°, 24.5° and 28.7° can be indexed to the (113), (024), (116), (214), (300) and (119) crystal facets of $K_2Zn_3[Fe(CN)_6]_2{\cdot}9H_2O$ (JCPDS no. 33-1061), which is consistent with the result of HRTEM, indicating the successful synthesis of the CC/KZHCF composite electrode. In addition, the XRD patterns of CC/KZHCF-1, CC/KZHCF-3 and CC/KZHCF-4 electrodes were also examined in Fig. S2.† Compared with the other three electrodes, the characteristic peaks of the CC/KZHCF-2 electrode are sharper, indicating its better crystallinity and thus was chosen as the representative for subsequent experiments.

### 3.2 Electrochemical evaluation of the CC/KZHCF electrode

The electrochemically active surface area (ECSA), which was determined in the electrolyte environment rather than the atmospheric environment for BET, is utilized to characterize the ion-accessible surface in electrochemical application.[36] As shown in Fig. 2a–c and Fig. S3,† the CC/KZHCF-2 electrode exhibits enhanced ECSA of 152.0 $m^2\ g^{-1}$, superior to that of CC/KZHCF-1 (141.7 $m^2\ g^{-1}$), CC/KZHCF-3 (144.9 $m^2\ g^{-1}$) and CC/KZHCF-4 (144.5 $m^2\ g^{-1}$). Evidently, the CC/KZHCF-2 electrode might provide abundant active sites that may facilitate ion storage during the electrochemical process and electrosorption of $Co^{2+}$ ions on the electrode surface, thereby achieving enhanced recovery efficiency. In addition, the $Fe^{II}/Fe^{III}$ redox properties of the CC/KZHCF electrodes were also evaluated by the CV curves in the electrolyte containing $Co^{2+}$, in which a significant pair of redox peaks appears in the CV curves for all the electrodes (Fig. 2d). A similar reduction peak at 0.55 V (*vs.* Ag/AgCl) was observed for $Co^{2+}$ ions intercalation in the investigated four CC/KZHCF electrodes, revealing the feasibility of KZHCF electrodes toward $Co^{2+}$ electrosorption. Also, the corresponding redox reaction can be described as follows (eqn (6)).[37] Note that the specific capacitance of the CC/KZHCF-2 electrode toward $Co^{2+}$ is higher than that of the other three electrodes. Hence, the CC/KZHCF-2 electrode is supposed to achieve the best recovery performance of $Co^{2+}$.

$$Zn_3[Fe^{III}(CN)_6]_2 + 2^{e-} + Co^{2+} \leftrightarrow CoZn_3[Fe^{II}(CN)_6]_2 \quad (6)$$

### 3.3 Electrosorption performance of $Co^{2+}$ ions on CC/KZHCF electrodes

The extraction efficiencies of $Co^{2+}$ on CC/KZHCF composite electrodes were evaluated under different operational con-

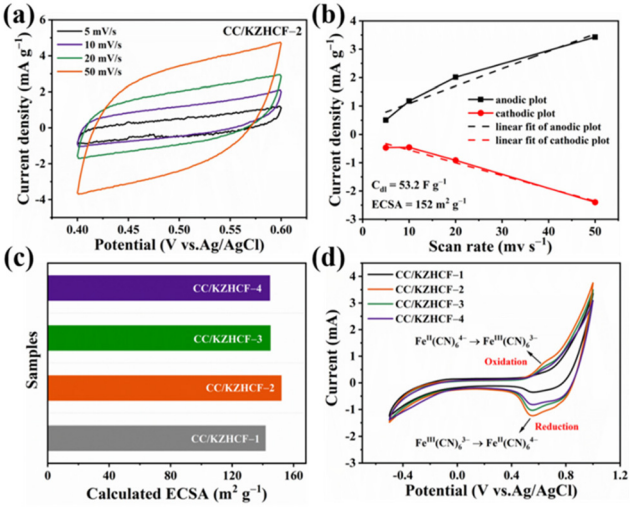


**Fig. 2** (a) CV curves of the CC/KZHCF-2 electrode at different scan rates between 0.40 and 0.60 V (*vs.* Ag/AgCl). (b) The corresponding cathodic and anodic charging current measured at 0.50 V (*vs.* Ag/AgCl) plotted as a function of scan rates. (c) Calculated ECSA values of different electrodes. (d) CV curves of different electrodes in 50 mM $Co^{2+}$ solution at a scan rate of 50 mV s$^{-1}$.

ditions. As compared to the other three composite electrodes, the CC/KZHCF-2 electrode exhibits higher extraction efficiency toward $Co^{2+}$ (Fig. 3a). Approximately 98.6% of $Co^{2+}$ (30 mg L$^{-1}$) was electrochemically adsorbed on the CC/KZHCF-2 electrode within 120 min. From the corresponding EDS elemental mapping after $Co^{2+}$ electrosorption (Fig. S4†), cobalt element was found to be uniformly distributed throughout the whole electrode surface, indicative of the successful electrosorption of $Co^{2+}$ by KZHCF. By contrast, the sorption efficiencies of $Co^{2+}$ on CC/KZHCF-1, CC/KZHCF-3 and CC/KZHCF-4 electrodes

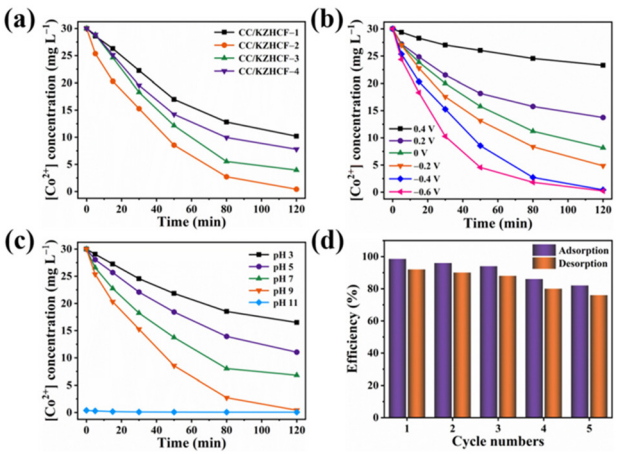


**Fig. 3** (a) $Co^{2+}$ electrosorption by different electrodes (voltage = −0.4 V (*vs.* Ag/AgCl), pH = 9). (b) Effect of working voltage (pH = 9) and (c) pH value (voltage = −0.4 V (*vs.* Ag/AgCl)) on $Co^{2+}$ electrosorption by the CC/KZHCF-2 electrode. (d) Reusability of the CC/KZHCF-2 electrode for 5 cycles.

were about 66.0%, 86.8% and 74.0%, respectively. Further, the electrosorption capacities of $Co^{2+}$ were calculated to be 116.5 mg g$^{-1}$, 130.9 mg g$^{-1}$, 69.3 mg g$^{-1}$ and 45.9 mg g$^{-1}$ for the respective CC/KZHCF-1, CC/KZHCF-2, CC/KZHCF-3 and CC/KZHCF-4. Evidently, the CC/KZHCF-2 composite electrode achieves excellent $Co^{2+}$ recovery performance in terms of the recovery efficiency and uptake capacity, which might be attributed to its high ECSA accessible and active adsorption sites.

The effect of the applied working potentials on the recovery efficiency of cobalt was also investigated. Considering that the side reaction of water electrolysis would occur below −0.8 V (*vs.* Ag/AgCl), the applied working potentials were selected from 0.4 V to −0.6 V (*vs.* Ag/AgCl).[38] As shown in Fig. 3b, the electrosorption efficiency of $Co^{2+}$ ions increased as the voltage becomes more negative, as reflected by 99.2% of the maximum value obtained at −0.6 V (*vs.* Ag/AgCl). Furthermore, the resulting CC/KZHCF-2 electrodes after $Co^{2+}$ adsorption between −0.4 V and −0.6 V (*vs.* Ag/AgCl) were subjected to XRD characterization. As demonstrated in Fig. S5,† unlike that for CC/KZHCF-2 under −0.4 V (*vs.* Ag/AgCl), two new peaks located at 43.2° and 50.3° were detected in the CC/KZHCF-2 under −0.6 V (*vs.* Ag/AgCl), which can be ascribed to the representative (111) and (002) diffractions of elemental Co (JCPDS no. 01-1625).[39] Thus, $Co^{2+}$ ions in the solution were reduced to $Co^0$ and deposited on the electrode surface under a potential of −0.6 V (*vs.* Ag/AgCl), while cobalt species were electrochemically adsorbed on the electrode surface in the form of ions under −0.4 V (*vs.* Ag/AgCl). Although a higher voltage might accelerate electron transfer, once $Co^{2+}$ ions are reduced to elemental $Co^0$, it is difficult for them to be oxidized into ions again and desorbed from the electrode surface into the solution. Moreover, the coating of cobalt on the KZHCF nanocubes is unfavorable for the subsequent cycling performance of the CC/KZHCF electrode. Hence, the optimal voltage toward cobalt recovery was set as −0.4 V (*vs.* Ag/AgCl).

Considering that $Co^{2+}$ ions exist in different forms under different pH conditions, the initial solution pH value is considered as another important factor affecting the cobalt recovery efficiency. As illustrated in Fig. 3c, a remarkable improvement in the cobalt recovery efficiency is observed from 45.0% to 98.6% with increasing pH from 3 to 9. The poor recovery efficiency under acidic condition might be ascribed to the fact that the electrode surface is slightly positively charged due to the protonation, which would repel the positively charged $Co^{2+}$ ions *via* the electrostatic repulsion effect.[40] Also, the higher adsorption capacity under weak alkalinity (*e.g.*, pH 9) can be explained by the formation of $Co(NH_3)_6^{3+}$ with 3.96 Å of hydrated radius, smaller than that of $Co^{2+}$ (4.23 Å) (eqn (7) and (8)).[41] As a result, $Co(NH_3)_6^{3+}$ with a smaller hydrated radius enters the KZHCF crystal lattice more easily, leading to enhanced recovery efficiency. Interestingly, it shows brown precipitation associated with $Co(OH)_2$ colloids under strong alkaline condition (*e.g.*, pH 11),[42] causing a decrease in the $Co^{2+}$ concentration in the solution, accompanied by the color variation of the electrolyte solution from light pink to colorless. These negatively charged colloids would adsorb $Li^+$ ions in the

 

solution, which is not conducive for the subsequent separation and recovery of $Co^{2+}$.

$$6NH_3 \cdot H_2O + Co^{2+} \leftrightarrow [Co(NH_3)_6]^{2+} + 6H_2O \quad (7)$$

$$4[Co(NH_3)_6]^{2+} + O_2 + 2H_2O \rightarrow 4[Co(NH_3)_6]^{3+} + 4OH^- \quad (8)$$

The cyclic performance and reusability of the CC/KZHCF-2 electrode were evaluated *via* 5 cycles of adsorption/desorption experiments, in which the spent electrode can be regenerated applying an oxidation potential of +1.5 V (*vs.* Ag/AgCl) in the pristine $KNO_3$ electrolyte for next round of $Co^{2+}$ electrosorption. Also, the adsorbed $Co^{2+}$ ions are desorbed from the electrode surface into the above solution for subsequent recovery. As exhibited in Fig. 3d, after 5 rounds, the adsorption and desorption efficiencies of $Co^{2+}$ decrease by 16.6% and 16.0%, respectively, indicating that most of the adsorbed $Co^{2+}$ ions can be desorbed from the electrode and the electrosorption capability can be successfully regenerated by switching to an oxidation state. In addition, the possible release of Zn and Fe ions during multiple electrochemical cycles was detected by ICP-OES to further verify the stability of CC/KZHCF. As shown in Fig. S6,† there was almost no loss of Zn and Fe ions in the initial two absorption and desorption processes, and a trace loss appears in the third cycle. After five cycles, the concentrations of Zn and Fe ions in the solution were 0.23 ppb and 0.41 ppb, respectively, indicating that the fabricated CC/KZHCF electrode possesses excellent structural stability during the electrochemical process. Further, the stability of the CC/KZHCF-2 electrode was examined by SEM and XRD characterization. As displayed in Fig. S7,† the electrode after $Co^{2+}$ desorption maintains the initial morphology with KZHCF nanocubes. In addition, the XRD pattern of the CC/KZHCF-2 electrode after $Co^{2+}$ desorption is basically consistent with that of the fresh electrode material, revealing its excellent structural stability and reusability.

The selective electrosorption of $Co^{2+}$ over $Li^+$ of the CC/KZHCF electrode was further investigated. It is well acknowledged that the alkaline ions with a smaller hydrated radius would enter into the lattice channels more easily. In our case, the hydrated radii follows the order: $Co^{2+}$ (4.23 Å) > $Co(NH_3)_6^{3+}$ (3.96 Å) > $Li^+$ (3.82 Å). Considering that monovalent ions have a lower energy than divalent ions,[43] a higher selectivity towards monovalent ions over divalent ions is achieved due to the dehydration energy. However, in our experiments, there is no change in the $Li^+$ concentration before and after cobalt extraction with the initial solution containing 30 mg $g^{-1}$ $Co^{2+}$ and 1.5 mg $g^{-1}$ $Li^+$ (Fig. S8a†). Herein, the CV curves were introduced to evaluate the electrochemical behaviors of the CC/KZHCF electrode in different electrolyte solutions (50 mM $Co^{2+}$ or $Li^+$). As depicted in Fig. S8b,† the reduction peaks at 0.55 V and 0.78 V (*vs.* Ag/AgCl) were observed for $Co^{2+}$ and $Li^+$ ions insertion, respectively, illustrating a relative smaller reduction potential for $Co^{2+}$ ions electrosorption in KZHCF in comparison with that of $Li^+$ ions. In other words, it is easier for $Co^{2+}$ insertion from the perspective of molecular dynamics due to its lower energy demand.[44] Such a selective electrosorption of $Co^{2+}$ over $Li^+$ might be attributed to the specific pseudocapacitive characteristics of KZHCF.

### 3.4 The possible mechanism of $Co^{2+}$ adsorption on the CC/KZHCF electrode

To gain more insight into the electrosorption mechanism of cobalt on the CC/KZHCF electrode, the chemical compositions and elemental states of CC/KZHCF before and after $Co^{2+}$ adsorption were probed by XPS spectroscopy. From the survey spectrum, a new characteristic peak assigned to Co 2p appears after $Co^{2+}$ adsorption as compared to the pristine CC/KZHCF electrode, indicating the successful extraction of cobalt by CC/KZHCF (Fig. S9†). The high-resolution spectrum of Fe 2p can be decomposed into two main peaks located at 721.4 and 708.6 eV, which can be assigned to the Fe $2p_{1/2}$ and Fe $2p_{3/2}$ spin-orbitals, respectively (Fig. 4a). The characteristic bands centred at 717.0 and 708.0 eV can be ascribed to the $Fe^{2+}$ state, while the other two peaks located at 721.4 and 708.6 eV can be assigned to the $Fe^{3+}$ state.[45] After $Co^{2+}$ extraction, the proportion of $Fe^{3+}$ decreases from 83.1% to 62.4%, while that of $Fe^{2+}$ increases from 10.6% to 27.8%. This result might be explained by the electrochemical transformation from $[Fe^{III}(CN)_6]^{3-}$ to $[Fe^{II}(CN)_6]^{4-}$. Similarly, the Co 2p spectrum after the electrosorption process is also verified in Fig. 4b, in which two main peaks at 797.1 and 781.3 eV correspond to the Co $2p_{1/2}$ and Co $2p_{3/2}$ spin-orbitals, respectively. Further, the Co 2p spectrum can be well fitted into several peaks associated with $Co^{2+}$ (802.0 and 785.4 eV), $Co^{3+}$ (797.1 and 781.3 eV) and satellite peaks (805.1 and 789.2 eV),[46] with the respective proportions of 27.8%, 56.1% and 16.1%. Thus, it can be concluded that most $Co^{2+}$ ions in the electrolyte are transformed to $[Co(NH_3)_6]^{3+}$ under weak alkaline condition. Based on the aforementioned XPS analyses, a possible electrosorption mechanism of $Co^{2+}$ on the CC/KZHCF electrode is proposed in Scheme 2. In the first step, $K^+$ cations are extracted from the KZHCF framework upon charging in the $KNO_3$ solution and leave large interstitial sites for the intercalation of cobalt ions. Then, $Co^{2+}$ ions in the electrolyte will combine with $NH_3 \cdot H_2O$ to form the $[Co(NH_3)_6]^{3+}$ complex and further migrate into the CC/KZHCF electrode under the action of an electric field. Subsequently, $[Co(NH_3)_6]^{3+}$ with a smaller hydrated radii than $Co^{2+}$ is easy to be inserted into the KZHCF framework to maintain charge neutrality. During the desorption process, the

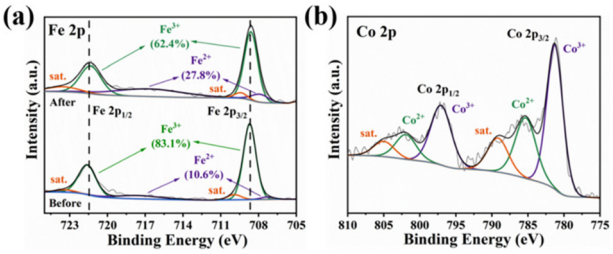


Fig. 4 High-resolution spectra of CC/KZHCF-2 before and after electrosorption: (a) Fe 2p and (b) Co 2p.

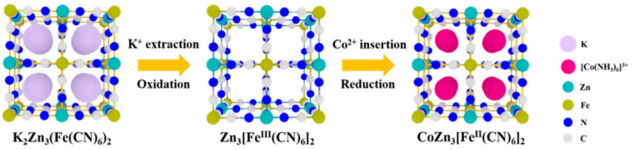


**Scheme 2** The electrosorption mechanism of $Co^{2+}$ on the CC/KZHCF-2 electrode.

$[Co(NH_3)_6]^{3+}$ ions are extracted from the interstitial sites for the exchange of $K^+$ ions in the pristine $KNO_3$ solution under an oxidation potential.

### 3.5 Simultaneous recovery of cobalt and lithium from spent $LiCO_2$

Apart from the selective electrosorption of $Co^{2+}$ from waste $LiCoO_2$ leaching, it is necessary to convert the extracted species into important industrial raw materials. Hence, after each cycle of $Co^{2+}$ electrosorption/desorption, the remaining solution containing $Li^+$ ions are collected for evaporation and concentration treatment, followed by the addition of solid $Na_2CO_3$ under continuous stirring and heating conditions. As a consequence, $Li_2CO_3$ is generated. Upon adjusting the pH solution to 13, the filtrate containing $Co^{2+}$ is collected, while $Co(OH)_2$ precipitation is obtained in a similar way. To verify the composition of the obtained $Li_2CO_3$, the powder was subjected to XRD characterization. As illustrated in Fig. 5a, several strong peaks located at 21.3°, 30.6°, 31.8°, 34.1° and 37.0° were detected, which can be attributed to the (110), (−202), (002), (−112) and (−311) diffractions of $Li_2CO_3$ (JCPDS no. 87-0728).[47] Additionally, an optical photograph intuitively reveals the white flake panorama of the obtained $Li_2CO_3$ powder (the inset in Fig. 5a). Likewise, the phase structure of the precipitated deep brown $Co(OH)_2$ powder was also confirmed by its XRD pattern (Fig. 5b). The diffraction peaks at 19.1°, 32.6°, 38.0°, 51.5° and 58.1° can be indexed to the (001), (100), (011), (012) and (110) facets of $Co(OH)_2$ (JCPDS no. 74-1057), respectively.[48] In addition, the purity of the recovered $Li_2CO_3$ and $Co(OH)_2$ products was detected by ICP-OES, in which $Li_2CO_3$ (1 g) and $Co(OH)_2$ (1 g) were separately subjected to digestion treatment in aqua regia ($HCl : HNO_3 = 3 : 1$) for one day, then the solution was diluted and the ion content was analyzed by ICP-OES. As displayed in Fig. S10,† the content of Li and Co was 0.186 g and 0.631 g, respectively. Accordingly, the purity of $Li_2CO_3$ and $Co(OH)_2$ was 99% and 99.6%, respectively. All these results mentioned above indicate that the combination of selective electrosorption and chemical precipitation might be applied for the effective recovery of cobalt and lithium from waste $LiCO_2$ cathode.

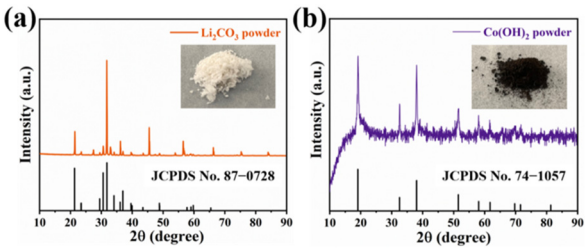


**Fig. 5** XRD patterns of the recovered (a) $Li_2CO_3$ and (b) $Co(OH)_2$ powders from waste $LiCoO_2$ cathode.

## 4. Conclusions

In summary, a free-standing CC/KZHCF composite electrode was successfully fabricated for the separation and recovery of $Co^{2+}$ and $Li^+$ from waste $LiCoO_2$ cathode. Benefiting from the open framework structure and specific selective pseudocapacitive behavior of KZHCF, the resultant CC/KZHCF composite electrode was capable of adsorbing electrochemically active $Co^{2+}$ with high efficiency and selectivity over $Li^+$ ions. By virtue of the electrochemically-mediated adsorption and desorption properties of KZHCF, the effective separation of $Co^{2+}$ and $Li^+$ was achieved, which can be further converted into important industrial raw materials (*e.g.*, $Co(OH)_2$ and $Li_2CO_3$) by means of chemical precipitation. It can be predicted that this work will pave the way for the sustainable recycling of the power battery industry.

## Data availability

The data supporting this article have been included as part of the ESI.†

## Conflicts of interest

There are no conflicts of interest to declare.

## Acknowledgements

This work was financially supported by National Natural Science Foundation of China (Grant No. 52173268 and 52371145), Anhui Provincial Natural Science Foundation (Grant No. 2308085QB73), and the HFIPS Director's Fund (Grant No. YZJJ-GGZX-2022-01).

## References

1 H. H. Liu, X. Zhang, H. R. Xu, W. Z. Ma, L. J. Wang, Z. H. Meng and F. Wang, $Li_2ZnTi_3O_8$ anode: design from material to electrode and devices, *Inorg. Chem. Front.*, 2023, **10**, 4943–4980.
2 X. B. Meng, Interface engineering of lithium metal anodes via atomic and molecular layer deposition, *Inorg. Chem. Front.*, 2024, **11**, 659–681.
3 W. Lv, J. W. Meng, Y. M. Li, W. J. Yang, Y. L. Tian, X. F. Lyu, C. E. Duan, X. L. Ma and Y. Wu, Inexpensive and eco-

friendly nanostructured birnessite-type δ-$MnO_2$: A design strategy from oxygen defect engineering and $K^+$ pre-intercalation, *Nano Energy*, 2022, **98**, 107274.

4 W. Lv, J. W. Meng, X. D. Li, C. Xu, W. J. Yang, S. Z. Duan, Y. M. Li, X. Ju, R. S. Yuan, Y. L. Tian, M. M. Wang, X. F. Lyu, P. Y. Pan, X. L. Ma, Y. Cong and Y. Wu, Boosting zinc storage in potassium-birnessite via organic-inorganic electrolyte strategy with slight N-methyl-2-pyrrolidone additive, *Energy Storage Mater.*, 2023, **54**, 784–793.

5 J. Chen, H. Y. Chen, S. Zhang, A. Dai, T. Y. Li, Y. Mei, L. S. Ni, X. Gao, W. T. Deng, L. Yu, G. Q. Zou, H. S. Hou, M. Dahbi, W. Q. Xu, J. G. Wen, J. Alami, T. C. Liu, K. Amine and X. B. Ji, Structure/Interface coupling effect for high-voltage $LiCoO_2$ cathodes, *Adv. Mater.*, 2022, **34**, 2204845.

6 W. Lv, Z. L. Shen, X. D. Li, J. W. Meng, W. J. Yang, F. Ding, X. Ju, F. Ye, Y. M. Li, X. F. Lyu, M. M. Wang, Y. L. Tian and C. Xu, Discovering cathodic biocompatibility for aqueous Zn–$MnO_2$ battery: An integrating biomass carbon strategy, *Nano-Micro Lett.*, 2024, **16**, 109.

7 S. M. Al-Salem, G. A. Leeke, M. S. El-Eskandarany and M. Van Haute, On the implementation of the circular economy route for E-waste management: A critical review and an analysis for the case of the state of Kuwait, *J. Environ. Manage.*, 2022, **323**, 116181.

8 J. J. Roy, S. Rarotra, V. Krikstolaityte, K. W. Zhuoran, Y. D. Cindy, X. Y. Tan, M. Carboni, D. Meyer, Q. Yan and M. Srinivasan, Green recycling methods to treat lithium-ion batteries E-waste: A circular approach to sustainability, *Adv. Mater.*, 2022, **34**, 2103346.

9 G. Yao, M. X. Lin, J. Yang, L. Z. Wei, H. L. Niu, Q. Q. Luo, F. C. Zheng and Q. W. Chen, Stabilizing $V_2O_3$ in carbon nanofiber flexible films for ultrastable potassium storage, *Inorg. Chem. Front.*, 2022, **9**, 1434–1445.

10 J. F. Xiao, J. Li and Z. M. Xu, Challenges to future development of spent lithium ion batteries recovery from environmental and technological perspectives, *Environ. Sci. Technol.*, 2020, **54**, 9–25.

11 T. Nshizirungu, M. Rana, Y. T. Jo and J. H. Park, Rapid leaching and recovery of valuable metals from spent lithium ion batteries (LIBs) via environmentally benign subcritical nickel-containing water over chlorinated polyvinyl chloride, *J. Hazard. Mater.*, 2020, **396**, 122667.

12 Y. H. Han, X. X. Yi, R. Wang, J. F. Huang, M. J. Chen, Z. Sun, S. H. Sun and J. C. Shu, Copper extraction from waste printed circuit boards by glycine, *Sep. Purif. Technol.*, 2020, **253**, 117463.

13 J. B. Qin, Z. Qu, H. Y. Chen, Z. H. Wang, Q. Han, Y. X. Zhang, H. Zhang, Y. D. Gao, Y. Zhang, X. Z. Wang and S. Y. Zhu, Pyrometallurgy treatment of electroplating sludge, emulsion mud and coal ash: $ZnAlFeO_4$ spinel separation and stabilization in calcium metasilicate glass, *J. Environ. Manage.*, 2022, **329**, 117101.

14 J. Lie and J. C. Liu, Closed-vessel microwave leaching of valuable metals from spent lithium-ion batteries (LIBs) using dual-function leaching agent: Ascorbic acid, *Sep. Purif. Technol.*, 2021, **266**, 118458.

15 H. M. Li, H. Zhang, J. F. Liu, Z. Z. Liu, H. M. Zhang, G. Z. Wang and Y. X. Zhang, Photo-enhanced precious metal recovery enabled by trithiocyanuric-linked covalent triazine frameworks, *Chem. Eng. J.*, 2024, **495**, 153494.

16 H. M. Li, M. X. Ye, Z. Fu, H. M. Zhang, G. Z. Wang and Y. X. Zhang, A freestanding, hierarchically porous poly (imine dioxime) membrane enabling selective gold recovery from e-waste with unprecedented capacity, *EcoMat*, 2022, e12248.

17 S. J. Li, C. W. Chen, H. J. Ge, X. Y. Guo, H. Xu, J. Zhang and Z. Y. Wu, Integration of galvanic reactions and engineered nanoconfinement in iron-copper nanocomposites for highly-efficient remediation of Cr(VI)-contaminated acidic/alkaline water, *Chem. Eng. J.*, 2024, **484**, 149533.

18 H. M. Li, M. X. Ye, Z. Z. Liu, Z. Fu, H. M. Zhang, G. Z. Wang and Y. X. Zhang, Selective Pt recovery from spent catalyst enabled by hierarchical porous poly(imine dioxime)/polyethylenimine composite membrane for recycled Pt/C catalyst, *Sep. Purif. Technol.*, 2023, **310**, 123125.

19 X. Y. Guo, Y. Zhang, H. J. Ge, J. Zhang, P. Q. Yang and Z. Y. Wu, Facile fabrication of 2D MXene loading Co-doped Prussian blue nanoparticles for ultrasensitive electrochemical assay of trace lead ions, *J. Electroanal. Chem.*, 2023, **935**, 117320.

20 Y. Yang, Q. G. Wang, S. Z. Xiong and Z. X. Song, Research progress on optimized membranes for vanadium redox flow batteries, *Inorg. Chem. Front.*, 2024, **11**, 4049–4079.

21 A. Hassanvand, G. Q. Chen, P. A. Webley and S. E. Kentish, A comparison of multicomponent electrosorption in capacitive deionization and membrane capacitive deionization, *Water Res.*, 2018, **131**, 100–109.

22 W. T. Chen, X. He, Z. K. Jiang, B. Li, X. Y. Li and L. Lin, A capacitive deionization and electro-oxidation hybrid system for simultaneous removal of heavy metals and organics from wastewater, *Chem. Eng. J.*, 2023, **451**, 139071.

23 D. I. Kim, G. Gwak, P. Dorji, D. He, S. Phuntsho, S. Hong and H. Shon, Palladium recovery through membrane capacitive deionization from metal plating wastewater, *ACS Sustainable Chem. Eng.*, 2017, **6**, 1692–1701.

24 X. Z. Zhou, A. X. Wang, X. Y. Zheng, D. F. Sun and Y. X. Yang, Uniformly anchoring $Sb_2O_5$ nanoparticles on graphene sheets via $Co^{2+}$-induced deposition for enhanced lithium/sodium-ion storage, *Inorg. Chem. Front.*, 2024, **11**, 4167–4178.

25 N. Kim, S. P. Hong, J. Lee, C. Kim and J. Yoon, High-desalination performance via redox couple reaction in the multichannel capacitive deionization system, *ACS Sustainable Chem. Eng.*, 2019, **7**, 16182–16189.

26 X. Su, K. J. Tan, J. Elbert, C. Rüttiger, M. Gallei, T. F. Jamison and T. A. Hatton, Asymmetric faradaic systems for selective electrochemical separations, *Energy Environ. Sci.*, 2017, **10**, 1272–1283.

27 L. Q. Deng, J. L. Qu, X. G. Niu, J. Z. Liu, J. Zhang, Y. R. Hong, M. Y. Feng, J. W. Wang, M. Hu, L. Zeng, Q. F. Zhang, L. Guo and Y. J. Zhu, Defect-free potassium manganese hexacyano-

ferrate cathode material for high-performance potassium-ion batteries, *Nat. Commun.*, 2021, **12**, 2167.

28 L. Niu, L. Chen, J. Zhang, P. Jiang and Z. P. Liu, Revisiting the open-framework zinc hexacyanoferrate: The role of ternary electrolyte and sodium-ion intercalation mechanism, *J. Power Sources*, 2018, **380**, 135–141.

29 K. Lu, B. Song, Y. X. Zhang, H. Y. Ma and J. T. Zhang, Encapsulation of zinc hexacyanoferrate nanocubes with manganese oxide nanosheets for high-performance rechargeable zinc ion batteries, *J. Mater. Chem. A*, 2017, **5**, 23628–23633.

30 H. Kim, H. H. Eom, Y. Kim, D. Harbottle and J. W. Lee, Reversible electro-mediated cesium ion removal using a zeolitic imidazolate framework derived zinc hexacyanoferrate composite, *Chem. Eng. J.*, 2022, **450**, 138029.

31 M. M. Cerrillo-Gonzalez, M. Villen-Guzman, C. Vereda-Alonso, J. M. Rodriguez-Maroto and J. M. Paz-Garcia, Acid leaching of $LiCoO_2$ enhanced by reducing agent. Model formulation and validation, *Chemosphere*, 2022, **287**, 132020.

32 B. He, P. Man, Q. C. Zhang, C. Wang, Z. Y. Zhou, C. W. Li, L. Wei and Y. G. Yao, Conversion synthesis of self-standing potassium zinc hexacyanoferrate arrays as cathodes for high-voltage flexible aqueous rechargeable sodium-ion batteries, *Small*, 2019, **15**, 1905115.

33 R. Z. Chen, H. Tanaka, T. Kawamoto, M. Asai, C. Fukushima, H. Na, M. Kurihara, M. Watanabe, M. Arisaka and T. Nankawa, Selective removal of cesium ions from wastewater using copper hexacyanoferrate nanofilms in an electrochemical system, *Electrochim. Acta*, 2013, **87**, 119–125.

34 Y. Y. Yuan, J. M. Xu, X. Y. Li, X. Li, X. C. Wang, X. J. Li and S. G. Dai, High-quality Prussian blue analogues $K_2Zn_3[Fe(CN)_6]_2$ crystals as a stable and high rate cathode material for potassium-ion batteries, *J. Alloys Compd.*, 2022, **923**, 166457.

35 Q. Q. Li, J. Wang, Y. H. Cheng and K. Chu, Zn nanosheets: An earth-abundant metallic catalyst for efficient electrochemical ammonia synthesis, *J. Energy Chem.*, 2021, **54**, 318–322.

36 M. X. Ye, C. Zhang, Z. Z. Liu, H. M. Li, Z. Fu, H. M. Zhang, G. Z. Wang and Y. X. Zhang, E-waste derived CuAu bimetallic catalysts supported on carbon cloth enabling effective degradation of bisphenol A via an electro-Fenton process, *Sep. Purif. Technol.*, 2023, **305**, 122507.

37 C. Y. Jiang, J. H. Ni and G. P. Jin, Magnetic potassium cobalt hexacyanoferrate nanocomposites for efficient adsorption of rubidium in solution, *Sep. Purif. Technol.*, 2022, **296**, 121383.

38 X. Wang, P. K. Cao, K. Zhao, S. Chen, H. T. Yu and X. Quan, Flow-through heterogeneous electro-Fenton system based on the absorbent cotton derived bulk electrode for refractory organic pollutants treatment, *Sep. Purif. Technol.*, 2021, **276**, 119266.

39 H. Feizi, R. Bagheri, Z. L. Song, J. R. Shen, S. I. Allakhverdiev and M. M. Najafpour, Cobalt/Cobalt oxide surface for water oxidation, *ACS Sustainable Chem. Eng.*, 2019, **7**, 6093–6105.

40 A. Amarray, S. El Ghachtouli, Y. Samih, M. Dahbi and M. Azzi, Enhancement of Cd(II) electrosorption using electrosorption process with manganese oxide nanomaterial electrodeposited, *Desalination*, 2022, **521**, 115307.

41 X. X. Long, R. Z. Chen, J. H. Tan, Y. F. Lu, J. X. Wang, T. J. Huang and Q. Lei, Electrochemical recovery of cobalt using nanoparticles film of copper hexacyanoferrates from aqueous solution, *J. Hazard. Mater.*, 2020, **384**, 121252.

42 R. Solís-Rodríguez, R. Pérez-Garibay, O. Alonso-González and D. Mendieta-George, Enhancing the arsenic adsorption by controlling the zeta potential of $Zn(OH)_2$ flocs, *J. Environ. Chem. Eng.*, 2021, **9**, 106300.

43 Y. S. Xu, H. J. Zhou, G. Z. Wang, Y. X. Zhang, H. M. Zhang and H. J. Zhao, Selective pseudocapacitive deionization of calcium ions in copper hexacyanoferrate, *ACS Appl. Mater. Interfaces*, 2020, **12**, 41437–41445.

44 T. H. Chen, D. V. Cuong, Y. Jang, N. Z. Khu, E. Chung and C. H. Hou, Cation selectivity of activated carbon and nickel hexacyanoferrate electrode materials in capacitive deionization: A comparison study, *Chemosphere*, 2022, **307**, 135613.

45 Z. Z. Li, C. S. Shen, Y. B. Liu, C. Y. Ma, F. Li, B. Yang, M. H. Huang, Z. W. Wang, L. M. Dong and S. Wolfgang, Carbon nanotube filter functionalized with iron oxychloride for flow-through electro-Fenton, *Appl. Catal., B*, 2020, **260**, 118204.

46 H. J. Zhou, H. C. Dong, J. H. Wang and Y. C. Chen, Cobalt anchored on porous N, P, S-doping core-shell with generating/activating dual reaction sites in heterogeneous electro-Fenton process, *Chem. Eng. J.*, 2021, **406**, 125990.

47 M. Shi, L. A. Diaz, J. R. Klaehn, A. D. Wilson and T. E. Lister, $Li_2CO_3$ Recovery through a carbon-negative electrodialysis of lithium-ion battery leachates, *ACS Sustainable Chem. Eng.*, 2022, **10**, 11773–11781.

48 J. J. Zhao, X. Qu, J. K. Qu, B. L. Zhang, Z. Q. Ning, H. W. Xie, X. B. Zhou, Q. S. Song, P. F. Xing and H. Y. Yin, Extraction of Co and $Li_2CO_3$ from cathode materials of spent lithium-ion batteries through a combined acid-leaching and electro-deoxidation approach, *J. Hazard. Mater.*, 2019, **379**, 120817.